Michigan State University

National Superconducting Cyclotron Laboratory

MEASUREMENTS OF THICK TARGET NEUTRON YIELDS AND SHIELDING STUDIES USING BEAMS OF ^{4}He, ^{12}C AND ^{16}O AT 155 MeV/NUCLEON FROM THE K1200 CYCLOTRON AT THE NATIONAL SUPERCONDUCTING CYCLOTRON LABORATORY

G.I. BRITVICH, A.A. CHUMAKOV, R.M. RONNINGEN, R.A. BLUE, and L.H. HEILBRONN

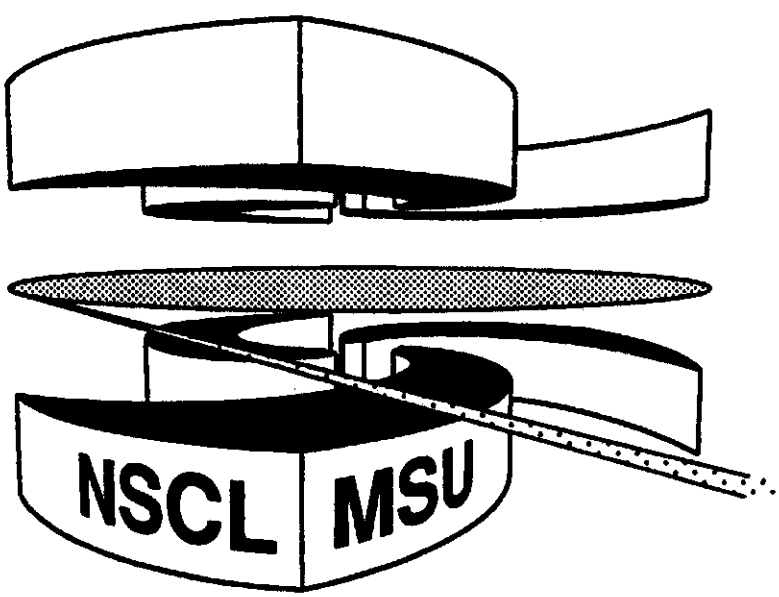

MSUCL-1092 MARCH 1998

Measurements of Thick Target Neutron Yields and Shielding Studies Using Beams of ^{4}He, ^{12}C and ^{16}O at 155 MeV/nucleon from the K1200 Cyclotron at the National Superconducting Cyclotron Laboratory

G.I. Britvich[1]
Superconducting Super Collider Laboratory
Waxahachee, TX 75165, USA

A.A. Chumakov
Institute for High Energy Physics
142284 Protvino, Russia

R.M. Ronningen, R.A. Blue
National Superconducting Cyclotron Laboratory
Michigan State- University, MI 48824, USA

And

L.H. Heilbronn
Lawrence Berkeley National Laboratory
Berkeley, CA 94720, USA

[1] Present address: Institute for High Energy Physics, 142284 Protvino, Russia

I. Introduction

The problem of shielding accelerators as sources of high-energy neutrons is important for both health and compliance reasons [1,2,3]. Complicating this problem, for high-energy, high-intensity heavy-ion accelerators, is the lack of data on neutron production from thick targets in the appropriate energy ranges.

Here, we present results from neutron flux measurements and shielding studies using the K1200 cyclotron at the National Superconducting Cyclotron Laboratory (NSCL). This cyclotron is based on a 280-ton superconducting magnet operating in the range of three to five Tesla. Typical maximum design energies are 200 MeV per nucleon for fully stripped N=Z ions through neon, and 25 MeV per nucleon, for ^{238}U ions [4]. The NSCL is planning an upgrade, by coupling its smaller, K500 superconducting cyclotron to the K1200 cyclotron [5]. This will significantly increase intensities of all ion beams, and significantly increase energies of the heavier ions. For example, ion beam currents of 1 particle-microampere are expected for ions to mass 40, and approximately 10^9 ions/sec are expected for 90 MeV/nucleon ^{238}U.

To provide needed information for shielding design, we measured neutron yields produced by 155 MeV/nucleon ^{4}He, ^{12}C, and ^{16}O ions stopping in a thick target of an alloy [6] of tungsten, nickel, and copper (below, we will call this alloy by its traditional name, "Hevimet"). Our study consists of measuring secondary neutron production, determining the dose equivalent behind thick concrete shielding, and studying the effect of local iron shielding above the target.

II. Experimental Arrangement

Measurements were carried out both inside and outside the concrete shielding of the Analysis Hall at the NSCL. A plan view of the beam line layout for the neutron shield studies is shown in Figure 1. The target was a solid cylinder of Hevimet. This target material was selected because Hevimet is used for many of the beam stops and Faraday

cups at the NSCL. The target diameter was 5.08 cm and the length was 5.093 cm. The ranges of the He, C, and O ions in Hevimet, when having 155 MeV per nucleon, are about 1.72 cm, 0.61 cm, and 0.46 cm, respectively. For reference, a proton's range in Hevimet, when its energy is 155 MeV, is about 1.78 cm. Thus, light charged particles produced with beam velocities will be stopped in the target.

Ions of ^{4}He, ^{12}C, and ^{16}O can be simultaneously produced in the NSCL's room temperature ECR ion source, from a mixture of He and CO_2 gases. When fully stripped, the ions are charge-to-mass analogs. The desired species can be selected by changing only the K1200 cyclotron frequency. However, we made separate experiments. The first used ^{12}C ions only, and the second used both ^{4}He and ^{16}O ions. In the latter experiment, we selected the desired ions by the appropriate cyclotron frequency.

Neutrons produced from the reactions between the ions and the Hevimet target penetrate the thick lateral concrete shielding to occupiable areas outside the Analysis Hall. The density of the concrete used at the NSCL is 2.4 g/cm^3. Table 1 gives, at the point of each measurement, the angle of detection with respect to the beam, the distance between the target and the detector, and the line-of-sight thickness of the concrete.

The vacuum chamber containing the target can be shielded locally by iron, to reduce the neutron flux which reaches the concrete walls. A local shadow shield of 25.4 cm-thick iron block can be moved into place over the target. The shield is "L-shaped", providing lateral and overhead shielding. Figure 2 is a vertical view of the general configuration, but shows only the overhead part of the shield. The data described in Section IV were obtained with the shield moved away from the vacuum chamber. In Section VII we describe measurements made with and without the local shielding in-place.

Measurements were also made on the "catwalk" (see Figures 2 and 3) above the shielding roof of the K1200 cyclotron. These are described in Section VIII. The measurement locations are shown in Figure 3.

III. Experimental Procedure

A. *Multisphere Spectrometry*

Energy spectra of neutrons emitted from the target were measured using a commercial Bonner-sphere spectrometer. This system includes spheres having diameters of 2, 3, 5, 8, 10 and 12 inches. Its detector is a 4-mm x 4-mm cylindrical LiI(Eu) scintillator, with 96% enrichment in ^{6}Li. The scintillator is optically coupled to a RCA 6199 photomultiplier (PM) by a Lucite light pipe (90-mm long, 12.7-mm diameter). The signals from PM were sent via a long coaxial cable to a main amplifier and multichannel analyzer. A background, resulting from the scintillator's response to background radiation, was subtracted from the peak containing the captured-neutron-induced alpha-particle events. A linear interpolation was used between the continuum values on either side of the alpha peak. The net number of counts in the peak per beam ion, the measured instrument response, was then determined.

B. *Spectral Unfolding Method*

To determine the neutron energy spectrum it is necessary to measure the detector response for a range of sizes of the moderating sphere surrounding the detector. If given the neutron energy spectrum, the measured instrument response may be predicted by folding the neutron energy spectrum with instrument responses to neutrons of known energies. In our case, we must solve the inverse problem. We measure the instrument response to an unknown neutron field, and then use known responses to "unfold" the neutron energy spectrum. We used the spectrum unfolding code, PREF, developed [7] at the Institute for High Energy Physics, Protvino, Russia. PREF uses a greatly modified version of the reconstruction method based on the Tikhonov's regularization [7].

C. *Bonner Sphere System Calibration*

The Bonner sphere system and associated electronics were calibrated in a relatively low-scatter area above the experimental halls at the NSCL. An unmoderated ^{239}Pu-Be source was used. The calibration procedure was essentially identical to the one described by Britvich *et al.* [8]. Spectral values of the integral flux, F, and the average neutron energy,

<E>, obtained from unfolding the bare Pu-Be calibration spectrum, F(E), are given in Table 2, where

$$F = \int_{8meV}^{12.6MeV} F(E)dE \text{ and } <E> = \int_{8meV}^{12.6MeV} E \times F(E)dE / F.$$

Integral fluence-to-dose conversion information is also given in Table 2. The spectrum-averaged fluence-to-dose-equivalent conversion factor, <h>, is defined by the International Organization for Standardization (ISO) [9] as the neutron-fluence to dose-equivalent conversion factor, h, averaged over the neutron source spectrum undisturbed by the irradiated object at the point of reference. For the calibration source:

$$<h> = \int_{8meV}^{12.6MeV} h(E) \times F(E)dE / F.$$

Similarly, the spectrum-averaged fluence-to-ambient-dose-equivalent conversion factor, <h*(10)>, is defined [9, 10] as the neutron-fluence to dose-equivalent conversion factor, h*(10), at a depth of 10 cm in a 30-cm diameter tissue equivalent sphere phantom, averaged over the neutron source spectrum undisturbed by the irradiated object at the point of reference. For the calibration source:

$$<h^*(10)> = \int_{8meV}^{12.6MeV} h^*(10)(E) \times F(E)dE / F.$$

In these equations, h(E) is the fluence-to-dose-equivalent conversion factor used in this work, defined by [9, 10], h*(10)(E) is the fluence-to-ambient-dose-equivalent conversion factor used in this work are recommended by [11] for neutrons having energies below 20 MeV, and by [12] for neutrons having energies above 20 MeV.

IV. Experimental Results

The experimental results for ^{4}He, ^{12}C and ^{16}O ions having energies of 155 MeV per nucleon and stopping in the thick Hevimet target are given in Tables 3, 4, 5a, and 5b, and in Figures 4, 5 and 6. The spectra measured at the emission angle $\theta = 94^{o}$ (at points 1, 9, and 9T, defined in Figures 1 and 3) were determined from data measured using all spheres. Spectral characteristics for $\theta = 34^{o}$, 49^{o}, and 59^{o}, were determined using only the 5-inch and 12-inch spheres.

The experimental neutron energy spectra, F(E) x E, inside the shielding, are shown in Figures 4, 5, and 6. *A priori* information about neutron spectra shapes was used in the unfolding process. We assumed a Maxwell distribution for thermal neutrons (8 meV < E_n < 50 meV). For neutron energies above 13.2 MeV, the shape is taken as the same as for the neutron spectra at $\theta = 90^o$ from 710 MeV ^{4}He ions stopping in an iron target [1].

The experimental neutron energy spectra, F(E) x E, outside of the shielding at 94°, is shown in Figure 7.

The responses of a 5-inch sphere k_5 as a function of <E> are shown in Figure 8, for typical neutron spectra behind the biological shields of nuclear-physics facilities [13]. The data set of 333 neutron spectra has been used to calculated k_5 as follows :

$$k_5 = \int_{E_{min}}^{E_{max}} R_5(E)\varphi(E)dE .$$

Here, $R_5(E)$ is the energy-dependent response of the detector, consisting of a 5-inch sphere and a 4-mm x 4-mm ^{6}LiI(Eu) scintillator, and $\varphi(E)$ is the literature spectrum, where

$$\int_{E_{min}}^{E_{max}} \varphi(E)dE = 1 .$$

E_{min} and E_{max} are the spectrum energy range bounds given in the literature. k_5 can be thought of as a "neutron flux meter". The values of k_5 measured in this work (see Table 5) are also shown in the figure. Similarly, responses of the 12-inch sphere, k_{12}, were calculated. These, along with our measurements, are shown in Figure 9.

The ratios of the 12-inch sphere-to-5-inch sphere responses, N_{12}/N_5, were calculated using the same data set as above. These are displayed in Figure 10, along with our measured values. The ratio obtained from the calibration data using a PuBe source (+) is also shown. The ratio N_{12}/N_5 can be used as a "<E_n> meter".

The average spectrum-weighted fluence-to-dose-equivalent conversion factor <h> is shown in Figure 11 as a function of <E>. The values of <h> are given for 330 spectra measured at nuclear physics facilities [13], and for 52 radioisotopic neutron-source spectra [14]. <h> is calculated using :

$$<h> = \int_{E_{min}}^{E_{max}} h(E)\varphi(E)dE \ ,$$

where φ(E) is the literature spectrum, with $\int_{E_{min}}^{E_{max}} \varphi(E)dE = 1$, E_{min} and E_{max} are the spectrum energy range bounds given in the literature. Values of <h> from our study (see Table 5), and h(E)-the energy dependence of the maximum dose-equivalent [8], are also shown.

V. Parameterizing the Neutron Production Cross Sections

Nakamura has studied the energy spectra of neutrons from ion beams having energies greater then 100 MeV per nucleon stopping in thick targets [16]. His phenomenological analysis gives production cross sections expressed by a simple formula consisting of three Maxwellian-like components, as follows:

$$\frac{d^2\sigma}{dEd\Omega} = \sum_{i=1}^{3} A_i(E/T_i^2(\theta))\exp(-E/T_i(\theta)). \qquad (1)$$

The first term corresponds to evaporation neutrons with nuclear temperature T_1= 2.2 MeV [2]; the intermediate component, having temperature T_2, corresponds to the pre-equilibrium emission, and the highest component, having temperature T_3, corresponds to the cascade process.

The neutron energy spectrum F(E) is given by:

$$F(E) = \varphi_{direct} + \varphi_{scattered} \ . \ (3)$$

Measurements using all Bonner spheres were made only at point 9, where θ = 94°. [The results for θ = 34°, 49°, and 59° are based on the response N(12") only, with sensitivity 6.5 n/cm^2/count for cascade neutrons only.] The measured spectra, F(E) x E, are shown in

Figures 4, 5, and 6. Contributions from scattered neutrons are observed to be large, as evidenced by the significant neutron flux in the thermal region.

Using the analytical form in Equation 1, we fit the spectra F(E), measured at point 9, for neutrons from the ^{4}He-induced reactions having energies greater than 2 MeV, obtaining

$$\varphi_{direct}(E) = E\left[10^{-2}\exp\left(-\frac{E}{2.2}\right)+2.4\times10^{-4}\exp\left(-\frac{E}{11.5}\right)+3.3\times10^{-6}\exp\left(-\frac{E}{36}\right)\right]. \quad (2)$$

Figures 4, 5, and 6 also show the fits to the data. The integral characteristics are given in the Table 5a.

Figure 12 shows the angular distributions of neutron yields, which we parameterize by

$$\varphi_{direct}(\theta) = C\times\exp(-\beta\theta)\ . \qquad (4)$$

The total neutron yield Y_{total} may be obtained using

$$Y_{total} = 2\pi\int_0^{\pi}\varphi(\theta)\sin\theta\,d\theta = 2\pi C\frac{(e^{-\beta\pi}+1)}{(\beta^2+1)}. \quad (5)$$

The values of b, C, and Y_{total}, calculated from the data shown in Figure 12, are given in Table 6. Comparisons of the present experimental results to other measurements are shown in Figure 13.

According to the data in Table 6, the ratios of total yields (4He:12C:16O) are 1:0.32:0.39. These can be compared to the ratios of the ion ranges, 1:0.35:0.27, and to the ratios of the number of nuclear interactions over the range, predicted by an energy-dependent geometrical model [17], 1:0.49:0.41. The ratio 4He:12C agrees well with the ratio of the ranges (assuming a 10% uncertainty in the total yields). However, the 4He:16O ratio agrees better with the ratio of interactions. If our data are correct (we cannot rule out beam current normalization uncertainties between the two experiments) an experiment using a heavier projectile would be interesting.

VI. Estimation of the Dose Equivalent Behind a Thick Shield

For ion beams exceeding energies of 100 MeV per nucleon it is possible [18] to use a phenomenological shielding model developed at high-energy proton accelerators, the

"Moyer model", to estimate the dose equivalent. In this model, it is assumed that the dose-equivalent due to neutrons penetrating a thick shield is proportional to the high-energy particle fluence, $h(E_p)$, and the amount of shielding present, by

$$H(E_p, \theta, d/\lambda) = \frac{h(E_p)}{r^2} \exp(-\beta\theta) \times \exp(-d(\theta)/\lambda). \quad (6)$$

Here, θ and r are the angle and distance, respectively, between the beam direction and the "neutron detector", β is a constant, $d(\theta)$ is the effective shielding thickness at angle θ, and λ is the attenuation length for neutrons in the shielding material.

In principle, it should be possible to modify Equation 6, for neutron production at high-energy heavy-ion accelerators. We have done so using our ^{4}He data. First, we note the angular distributions have a shallow slope. Then, in Equation 5, $\frac{(e^{-\beta\pi}+1)}{(\beta^2+1)} \approx 1$, and $Y_{total} = 2\pi C$, as for a point source. Secondly, the maximum dose equivalent is when $\theta = \frac{\pi}{2}$. This condition allows one to estimate the maximum lateral shielding necessary for some desired dose-equivalent outside of the shielding.

From these two considerations it follows that dose equivalent behind the shielding can be estimated by

$$H(r, \frac{d}{\lambda}) = \frac{0.5 \times Y_{total} \times < h >}{4\pi r^2} \exp(-\frac{d}{\lambda}), \quad (7)$$

where $0.5Y_{total}$ is the neutron yield from the intermediate-energy component (pre-equilibrium emission, with effective temperature T_2) and the high-energy component (cascade process, with effective temperature T_3). We have also used the fluence-to-dose equivalent conversion factor $<h> = 4.5 \times 10^{-10}$ Sv/neutron/cm^2, obtained from Figure 12, at $<E> = 30$ MeV, the average neutron energy for φ_{casc}.

We estimate λ, using Equation 7 and our experimental results for point 1, where H(point 1, ^{4}He ions) = 1.69×10^{-19} Sv/ion, r = 403 cm, d = 308 g/cm^2, and $Y_{total} = 4.9$. We obtain λ = 38 g/cm^2. In our case, λ = 38 g/cm^2 corresponds to $<E_n> = 2T_3 \sim 70$ MeV for highest

component T_3 of the cascade process. This result shows good agreement with those given by ref. [19], where λ = 36 g/cm^2 for E_n = 41.5 MeV, and λ = 46 g/cm^2 for E_n = 64.3 MeV.

Finally,

$$H(r,d) = \frac{0.5 \times Y_{total} \times 4.5 \times 10^{-10}}{4\pi r^2} \exp(-\frac{d}{38}) \text{ [Sv / ion]}, \quad (8)$$

VII. Estimation of the Effect of Local Iron Shielding

A vertical view of the beam line for the local-iron-shielding experiment is shown in Figure 2. Pre-equilibrium and cascade neutrons from the Hevimet target penetrate the local iron shield, and the concrete shielding of the Analysis Hall roof, where the measurements were made. The local shield consists of iron block, having a thickness of 25.4 cm. The total thickness of the concrete, in two layers of beams that make up the roof shielding, is 137.2 cm.

We refer to the point on the roof where the measurements were made as point 8, when the local shield was rolled back, leaving just concrete shielding between the target chamber and the detector. We refer to this point as 8*, when the shield was in place. Only the integral characteristics of the field were measured, using the 5-inch and 12-inch spheres. These are:

(1) the fluence-weighted average neutron energy <E>, estimated by comparing the measured ratio N(12")/N(5") to the dependence of this ratio on <E_n>, shown in Figure 10;

(2) the neutron fluence F, estimated from the dependence of the ratio N(5")/F on <E_n>, shown in Figure 9;

(3) the average spectrum-weighted fluence-to-dose-equivalent conversion factor <h>, estimated from the dependence of H=F<h> on <E_n>, shown in Figure 11; and

(4) the neutron dose equivalent H, from the dependence of H/N(12") on <E_n>, shown in Figure 11.

Table 9 summarizes results. Dose equivalents were calculated using Equation 8, based on experimental results for point 1, which is also at about 90°. Tables 9 and 10 show the following:

(1) The value for <E> at point 8 is about 10 times smaller than for point 1. This is because that the local iron shield, even when moved back from the target, scatters neutrons into point 8, contributing to the low energy portion of the spectrum.

(2) Moving the local shield over the target further reduces the average energy by about a factor of two, although the flux remains nearly the same. Because of the energy shift, the <h> and the dose equivalent are reduced by a factor of 1.4 to 1.5. The calculation of the scattered neutrons shows that the dose equivalent should be reduced by nearly a factor of four.

VIII. Estimation of the Dose Equivalent Above the Steel (Iron) Roof Shielding of the K1200 Cyclotron

The K1200 cyclotron roof shielding consists of two moveable iron slabs, each having a thickness of 30.48 cm. These slabs roll on stationary iron slabs (see Figure 3), which are also 30.48-cm thick. This thinner iron shielding was specified to allow access for the facility crane. Because iron "leaks" low energy neutrons, it was of interest to measure the neutron spectrum above this roof. As before, point 1 is used for reference. Neutron spectral characteristics were measured at eleven points. Those points, denoted with "T" (1T through 11T), are above (at approximately 90° to the beam direction) the K1200 cyclotron, as shown in Figure 2. This area is secured from entrance by personnel during cyclotron operations.

Only the integral characteristics of the fields were measured, using the 5-inch and 12-inch spheres as described in Section VI. The results are given in Tables 4, 5, 7, and 8, and are shown in Figures 8, 9, 10 and 11.

The neutron spectra above the shielding can be described by :

(1) the high energy leakage neutron component

$$\varphi_{casc.} = E \times [C_2 \exp(-\frac{E}{T_2}) + C_3 \exp(-\frac{E}{T_3})], where$$
$$T_2 \approx 10 MeV, T_3 \approx 30 MeV;$$

(2) a quasi-Maxwellian "evaporation" component of the spectrum with the effective temperature about 2 MeV;

(3) a 1 / E component of the spectrum from the air-scattered neutrons (below 0.1 MeV);

(4) an intermediate-energy neutron peak behind the thick iron shield which is related to the neutron-iron interaction cross-section minimum (in the vicinity of the neutron energy of 24 keV); and

(5) an additional contribution from the intermediate energy neutrons from the communication penetrations of the shield (below 1 keV). This has been observed in the analysis of neutron spectra behind the biological shields at other nuclear installations [20].

The data show that the iron shielding reduces the average energy of the neutrons by a factor of about 56, but the flux is increased by "low-energy leakage" and scattering. Hence, the dose-equivalent per ion is not much reduced. This iron shielding should be supplemented by the addition of lighter mass shielding, to reduce the number of low-energy neutrons that penetrate this iron shield.

IX. Comparison between the Method of Reconstructed Spectra and the 6-Spheres Method

The integral values of neutron fields (see Table 2 and 5) have been calculated by the unfolding method to reconstruct the spectra of these fields. We also obtained them using the 6-spheres method [8, 21]. In this method one takes

$$F = R \sum_{i=1}^{6} A_i \times N_i \qquad < E >= P \sum_{i=1}^{6} B_i \times N_i$$

$$H = K \sum_{i=1}^{6} B_i \times N_i \qquad H^*(10) = L \sum_{i=1}^{6} C_i \times N_i$$

where N_i is the count rate from neutrons as measured by the ^{6}LiI(Eu) detector with I-th moderator; R,P,K,L are the normalization factors; A_i, D_i, B_i, C_i are the positive fitting parameters such that:

$$\sum_{i=1}^{6} A_i \times \eta_i(E) \approx const \qquad \sum_{i=1}^{6} D_i \times \eta_i(E) \approx E$$

$$\sum_{i=1}^{6} B_i \times \eta_i(E) \approx h(E) \qquad \sum_{i=1}^{6} C_i \times \eta_i(E) \approx h^*(10)(E)$$

where η_i(E) are the responses of the Bonner sphere spectrometer.

The integral values calculated from unfolded spectra, and those obtained with the 6-spheres method, are given in the Table 10. The two methods show good agreement, at the ~ 10% level for F, H and H*(10), and at ~25% level for <E>.

X. Conclusions

The results obtained in this work are useful for a determination of the neutron source-term, and for a determination of dose-equivalents. Both are valuable for the shielding design studies at the NSCL.

We learned that local iron shielding inside of a vault's concrete shielding significantly reduces the average neutron energy observed outside of the concrete shielding. However, neutron scattering from local shielding can increase the observed flux outside of the vault.

We also observed that a vault roof constructed of iron greatly reduces the average energy of the neutrons, but the flux is increased by "low-energy leakage" and scattering. We found the dose-equivalent per ion is not much reduced. This pointed out the need to supplement this iron shielding with lighter mass shielding, to reduce the number of low-energy neutrons that penetrate the iron shield.

Our results may prove useful to other accelerator facilities producing heavy-ion beams with similar energies.

Acknowledgements

This work was supported by the National Science Foundation under the grants PHY-9214992 and PHY-9528844 (NSCL), NASA Grant L14230C through the U.S. Department of Energy under Contract No. DE-AC03076SF00098 (LNBL), and by Universities Research Associates, Inc., which was supported by the U.S. Department of Energy under Contract No. DE-AC3589ER40486 (SSCL).

We thank Drs. N. Mohkov and G. Stapleton for useful discussions, and for their support of this research. We also thank the NSCL's Operations Department for providing the ion beams. Finally, we thank Mr. Charles Nelson and the Indiana University Cyclotron Facility for loaning us their Bonner-sphere spectrometer.

Table 1: Location of Measurement Points in the Plane of Figure 1.

Point	Geometry		Thickness t of concrete*) [g/cm2]
	angle θ [degree]	distance R from target [cm]	
1	94	403	308
2	82	446	341
3	73	499	471
4	65	568	560
5	54	726	716
6	49	862	863
7	44	1055	1057
9	94	121	0
10	59	176	0
11	49	248	0
12	34	402	0

*) density = 2.4 g/cm^3

Table 2: Integral characteristics of the ^{239}Pu-Be neutron spectrum at a distance of 777-mm (center of detector-to-center of source).

METHOD	INTEGRAL VALUES			
	F [n /cm2/ s]	<E> [MeV]	<h> x10-10 [Sv×cm2]	<h*> x10-10 [Sv×cm2]
Ref.[6]	115.0 *) +/- 5%	4.157	3.642	3.699
Spectra unfolded with *a priori* **)	$115.0^{+5.8}_{-5.2}$	$4.157^{+.112}_{-.093}$	$3.642^{+.008}_{-.006}$	$3.699^{+.015}_{-.013}$

*) certificate of calibration: source strength = 8.73x10^6 neutrons/second (Pu-Be M-830 Monsanto Research Corp.)

**) shape of the spectrum from Ref. 8 with calibration*)

Table 3: Response N(j) of the Bonner sphere j for the neutron spectra (counts per incidence ion in the thermal peak) and for the Pu-Be source (counts per second in the thermal peak).

Sphere Dia. [inch]	Pu-Be	Point 1		Point 9			Point 9T
		^{4}He	^{12}C	^{4}He	^{12}C	^{16}O	^{4}He
2"	7.83E-01	1.92E-10	5.98E-11	3.82E-06	1.42E-06	2.07E-06	2.97E-09
3"	4.33E-00	2.12E-10	8.99E-11	1.16E-05	3.02E-06	4.89E-06	5.19E-09
5"	1.45E 01	2.32E-10	1.27E-10	2.02E-05	4.72E-06	7.60E-06	6.06E-09
8"	1.99E 01	1.10E-10	6.55E-11	9.80E-06	3.48E-06	5.56E-06	1.88E-09
10"	1.83E 01	7.10E-11	5.77E-11	5.35E-06	1.99E-06	2.85E-06	8.50E-10
12"	1.43E 01	4.52E-11	3.57E-11	4.47E-06	1.33E-06	1.59E-06	3.09E-10

Table 4:Response N(5") and N(12") of the Bonner sphere (counts per incidence ion in the thermal peak) at the points of measurement.

Point	Ions					
	^4He		^{12}C		^{16}O	
	Sphere diameter					
	5"	12"	5"	12"	5"	12"
2			1.10E-10			
3			1.05E-10	2.93E-11		
4			8.95E-11			
5			5.82E-11	8.01E-12		
6			3.64E-11			
7			2.65E-11			
8			7.71E-11	1.01E-11		
8*)			7.91E-11	7.60E-12		
10	1.32E-05	2.53E-06	3.57E-06	8.34E-07	4.79E-06	1.15E-06
11	7.70E-06	1.31E-06	2.36E-06	5.14E-07	3.15E-06	6.39E-07
12	3.14E-06	5.67E-07	1.07E-06	1.66E-07	1.48E-06	2.41E-07
1T	2.30E-09					
2T	3.42E-09					
3T	3.88E-09					
4T	3.76E-09					
5T	3.21E-09					
7T	1.62E-09					
10T	6.13E-09					
11T	4.24E-09					

*) with local iron shield.

Table 5a: Integral characteristics of the neutron spectra. The F, H and $H^*(10)$ are normalized to 1 incident ion.

	Point 1		Point 9			Point 9T
	^{4}He	^{12}C	^{4}He	^{12}C	^{16}O	^{4}He
F neutron/cm^2	1.28E-09	6.51E-10	8.34E-05	2.55E-05	3.94E-05	2.51E-08
<E> MeV	3.17E-00	3.11E-00	4.98E-00	4.60E-00	3.03E-00	5.70E-02
<h> Svxcm^2	1.32E-10	1.91E-10	1.91E-10	2.01E-10	1.81E-10	2.91E-11
<h*(10)> Svxcm^2	1.37E-10	2.01E-10	1.97E-10	2.04E-10	1.82E-10	2.27E-11
H Sv	1.69E-19	1.24E-19	1.59E-14	5.12E-15	7.13E-15	7.30E-19
H*(10) Sv	1.75E-19	1.31E-19	1.64E-14	5.20E-15	7.17E-15	5.70E-19
k5 neutron/count	5.52E-00	5.13E-00	4.13E-00	5.40E-00	5.18E-00	4.14E-00
k12 Sv/count	3.74E-09	3.47E-09	3.56E-09	3.85E-09	4.48E-09	2.36E-09

$$\mathbf{F} = \int_{8meV}^{126MeV} F(E)dE, <\mathbf{E}> = \frac{\int_{8meV}^{126MeV} F(E)\times EdE}{\int_{8meV}^{126MeV} F(E)dE}$$

$$<h> = \frac{\int_{8meV}^{126MeV} F(E)\times h(E)dE}{\int_{8meV}^{126MeV} F(E)dE}, <h^*> = \frac{\int_{8meV}^{126MeV} F(E)\times h^*(10)(E)dE}{\int_{8meV}^{126MeV} F(E)dE}$$

$$H = F\times <h>, H^*(10) = F\times <h^*(10)>, k_5 = \frac{F}{N(5")}, k_{12} = \frac{H}{N(12")}$$

Table 5b: Integral characteristics of the $\varphi_{casc.}(E)$ neutron spectra in the point 9 for ^{4}He, ^{12}C, and ^{16}O. The F, H and $H^{*}(10)$ are normalized to 1 incident ion.

	^{4}He	^{12}C	^{16}O
F neutron/cm ^{2}	2.38E-05	8.36E-06	8.23E-06
<E> MeV	1.38E 01	1.37E 01	1.37E 01
<h> Sv$_{x}$cm^{2}	4.03E-10	4.02E-10	4.02E-10
<h*(10)> Sv$_{x}$cm^{2}	4.21E-10	4.20E-10	4.20E-10
H Sv	1.05E-14	3.36E-15	3.31E-15
H*(10) Sv	1.08E-14	3.52E-15	3.46E-15
k_{12} Sv/count	2.62E-09	2.53E-09	2.08E-09
kf_{12} neutron/count *)	6.5E-00	6.3E-00	5.2E-00

*) $$kf_{12} = \frac{\int_{-1keV}^{126MeV} \varphi_{casc.}(E)dE}{N(12")}$$

Table 6: The thick-target neutron yields for ^{4}He, ^{12}C and ^{16}O ions having 155 MeV per nucleon.

Angle θ [degrees]	Neutron Yield f(θ) *) [neutron / sr x incident ion]		
	^{4}He	^{12}C	^{16}O
34	.596	.169	.202
49	.524	.199	.204
59	.509	.162	.185
94	.425	.122	.121
C and β values, from fitting to Equation 4:			
C [n / incident ion]	.80	.26	.29
β [sr^{-1}]	.49	.51	.51
Total neutron yields Y_{total}, from Equation 5 [neutrons / incident ion]:			
	4.90	1.56	1.74

Table 7: Integral characteristics of the neutron fields above the K1200 cyclotron roof for ^{4}He ions. F and H are normalized to 1 incident ion.

Point	<E> [MeV]	k_5 [neutron/count]	<h> [Svxcm^2]	F [neutron/cm^2]	H [Sv]
1	3.17E-00	5.52E-00	1.32E-10	1.28E-09	1.69E-19
1T	5.70E-02	4.14E-00	2.91E-11	9.52E-09	2.77E-19
2T	5.70E-02	4.14E-00	2.91E-11	1.42E-08	4.12E-19
3T	5.70E-02	4.14E-00	2.91E-11	1.61E-08	4.67E-19
4T	5.70E-02	4.14E-00	2.91E-11	1.56E-08	4.53E-19
5T	5.70E-02	4.14E-00	2.91E-11	1.33E-08	3.87E-19
7T	5.70E-02	4.14E-00	2.91E-11	6.71E-09	1.95E-19
9T	5.70E-02	4.14E-00	2.91E-11	2.51E-08	7.30E-19
10T	5.70E-02	4.14E-00	2.91E-11	2.54E-08	7.39E-19
11T	5.70E-02	4.14E-00	2.91E-11	1.76E-08	5.11E-19

Table 8: Integral characteristics of the neutron fields behind MSU cyclotron for ^{12}C ions. F and H are normalized to 1 incident ion.

Point	<E> [MeV]	k5 [neutron/count]	<h> [Svxcm^2]	F [neutron/cm^2]	H [Sv]
1	3.11E-00	5.13E-00	1.91E-10	6.51E-10	1.24E-19
2	3.11E-00	5.13E-00	1.91E-10	5.64E-10	1.08E-19
3	3.11E-00	5.13E-00	1.91E-10	5.39E-10	1.03E-19
4	1.00E-00	4.20E-00	1.70E-10	3.76E-10	6.39E-20
5	3.50E-01	4.14E-00	8.00E-11	2.41E-10	1.93E-20
6	3.00E-01	4.14E-00	7.50E-11	1.51E-10	1.13E-20
7	3.00E-01	4.14E-00	7.50E-11	1.10E-10	8.23E-21
8	3.00E-01	4.14E-00	7.50E-11	3.19E-10	2.39E-20
8*	1.60E-01	4.14E-00	5.20E-11	3.27E-10	1.70E-20

Table 9: Integral characteristics of the neutron fields outside of the K1200 cyclotron shielding at points 8 and 8* for ^{12}C ions. F and H are normalized to 1 incident ion.

Point	<E> [MeV]	F x10^{-10} [neutrons/cm^2]	H x10^{-22} [Sv]		
			Experiment		Calculated
			Using the energy dependence of <h>	At one average energy	
8	3.00E-01	3.19	239	283	20
8*	1.60E-01	3.27	170	190	5.1*)
Ratio:	1.9	~1	1.4	1.5	3.9

*) with $\exp(-t_{Fe}/\lambda_{Fe})$, where λ_{Fe}=18.6 cm [20].

Table 10: The integral values of neutron fields obtained by means of the reconstructed spectra (*s*) and with help of the 6-spheres method (f). The ratio f/s was obtained without using the spectral data at point 9T.

Point	Ion	Method	F [n/cm^2/ion]	<E> [MeV]	H [Sv/ion]	H*(10) [Sv/ion]
1	4He	s	$\left(1.28^{+.09}_{-.13}\right)\times10^{-9}$	3.17±.80	(1.69±.20)×10^{-19}	(1.75±.21)×10^{-19}
1	4He	f	(1.19±.09)×10^{-9}	1.95±.23	(1.77±.21)×10^{-19}	(1.76±.21)×10^{-19}
1	12C	s	$\left(6.51^{+.60}_{-.72}\right)\times10^{-10}$	3.11±.78	(1.24±.15)×10^{-19}	(1.31±.16)×10^{-19}
1	12C	f	(6.50±.55)×10^{-10}	2.67±.35	(1.30±.17)×10^{-19}	(1.29±.17)×10^{-19}
9	4He	s	$\left(8.34^{+.59}_{-.84}\right)\times10^{-5}$	$4.98^{+1.07}_{-1.09}$	$\left(1.59^{+.33}_{-.19}\right)\times10^{-14}$	$\left(1.64^{+.37}_{-.21}\right)\times10^{-14}$
9	4He	f	(9.48±.75)×10^{-5}	2.43±.28	(1.75±.21)×10^{-14}	(1.74±.22)×10^{-14}
9	12C	s	$\left(2.55^{+.24}_{-.30}\right)\times10^{-5}$	$4.60^{+1.37}_{-2.19}$	$\left(5.12^{+.79}_{-.76}\right)\times10^{-15}$	$\left(5.20^{+1.01}_{-.87}\right)\times10^{-15}$
9	12C	f	(2.36±.20)×10^{-5}	2.74±.36	(4.84±.64)×10^{-15}	(4.86±.64)×10^{-15}
9	16O	s	$\left(3.95^{+.34}_{-.52}\right)\times10^{-5}$	$3.03^{+1.12}_{-1.81}$	(7.13±1.08)×10^{-15}	$\left(7.17^{+1.46}_{-1.11}\right)\times10^{-15}$
9	16O	f	(3.59±.28)×10^{-5}	2.28±.26	(6.22±.68)×10^{-15}	(6.19±.70)×10^{-15}
$\left(\frac{f}{s}\right)\pm\sigma$			0.96±.11	0.68±.18	1.00±.11	0.97±.11
9T	4He	s	$\left(2.51^{+.94}_{-1.20}\right)\times10^{-8}$	$0.057^{+.123}_{-.023}$	$\left(7.30^{+.82}_{-.49}\right)\times10^{-19}$	$\left(5.70^{+1.17}_{-.60}\right)\times10^{-19}$
9T	4He	f	(2.48±.22)×10^{-8}	0.480±.056	(1.21±.14)×10^{-18}	(1.20±.14)×10^{-18}

References

1. R.A. Cecil *et al.*, "Neutron angular and energy distributions from 710-MeV alphas stopping in water, carbon, steel, and lead, and 640-MeV alphas stopping in lead", Phys. Rev. C **21**, 2471- 2484 (1980).

2. T. Kato and T. Nakamura, "Estimation of neutron yields from thick target by high energy ^{4}He ions for the design of shielding for a heavy ion medical accelerator", Nucl. Instr. Meth. Phys. Res. **A311**, 548-557 (1992).

3. J. Krishnamoorty *et al.*, "Neutron shielding calculations for the K1200 cyclotron at the National Superconducting Cyclotron Laboratory", Proceeding 8th Intern. Conf. on Radiation Shielding, Arlington, Texas USA, 1994, pp. 650-653.

4. J.A. Nolen, Jr., "Commissioning experience with the largest superconducting cyclotron, the NSCL K800", Nucl. Instr. Meth. Phys. Res. **B40/41**, 870-873 (1989).

5. "The K500⊗K1200, A Coupled Cyclotron Facility at the National Superconducting Cyclotron Laboratory, Michigan State University. Scientific Justification and Technical Specifications for a Cost-Effective Upgrade of the NSCL Facility", MSUCL-939, July, 1994.

6. HD18, by Mi-Tech Metals, Inc., 1340 N. Senate Ave., Indianapolis, IN 46202; HD18 is 95% tungsten, 3.5% Ni, and 1.5% copper, and has a density of 18 g/cm^3.

7. E.A. Belogorlov and V.P. Zhigunov, "Interpretation of the solution to the inverse problem for the positive function and the reconstruction of neutron spectra", Nucl. Instr. Meth. Phys. Res. **A235**, 146-163 (1985).

8. G.I. Britvich *et al.*, "Spectra and integral values of reference neutron fields from radionuclide neutron sources", IHEP preprint, IHEP 90-48, Protvino, 1990.

9. International Organization for Standardization, "Neutron reference radiation for calibrating neutron measuring devices used for radiation protection purposes and for determining their response as a function of neutron energy", Geneva: ISO; International Standard ISO/DIS, 8529 (1989).

10. ICRP Recommendation of the International Commission on Radiological Protection, Publication 51, Oxford: Pergamon Press, 1987.

11. E.A. Belogorlov *et al.*, "Depth dose and depth dose equivalent data for neutrons with energy from thermal up to several TeV", Nucl. Instr. Meth. **199,** 563-572 (1982).

12. A.V. Sannikov and E.N. Savitskaya, "Ambient dose and ambient dose equivalent conversion factors for high-energy neutrons", CERN preprint, CERN/TIS-RP/93-14/PP/ (1993)

13. G.I. Britvich *et al.*, Typical neutron spectra in work and auxiliary environments of reactor, accelerators and installations with isotopes (In Russian), Report IHEP, Dep. of Radiation Research, Protvino, (1985).

14. R.V. Griffith *et al.*, "Compendium of neutron spectra and detector responses for radiation protection purposes", IAEA Technical Report Series No. 318 (Vienna: IAEA) (1990).

15. M.A. Buckner and C.S. Sims, "Neutron dosimetric quantities for several radioisotopic neutron sources", Health Phys. **63,** 352-355 (1992).

16. T. Nakamura, "Neutron energy spectra produced from thick targets by light-mass heavy ions", Nucl. Instr. Meth. Phys. Res. **A240**, 207-215 (1985).

17. L. W. Townsend and J. W. Wilson, Phys. Rev. C **37**, 892 (1988).

18. K. Hayashi *et al.*, "Accelerator shielding benchmark analysis and future items to be solved", Meeting on Shielding Aspects of Accelerators, Targets and Irradiation Facilities, Arlington, Texas, USA, April 28-29, 1994. L.E. Moritz, "Review of proton accelerator shielding problems", *ibid.*

19. Y. Sakamoto *et al.*, "Shielding experiments with quasi-monoenergetic neutrons between 15 and 90 MeV at 90 MV AVF cyclotron facility TIARA", Proceeding 8th Intern. Conf. on Radiation Shielding, Arlington, Texas USA, 1994, pp. 809-815.

20. G. I. Britvich and A.A. Chumakov, Reference fields superposition method for dosimetric apparatus calibration to operate within the neutron radiation fields, IHEP preprint, IHEP 93-66, Protvino, 1993.

21. J.D. Nachtigall and F. Rohlaff, "Verfahren zur Messung der Flußdichten und Dosisleistungsäquivalente von Neutronen im Energiebereich Zwischen Thermische Energie und 50 MeV", Nucl. Instr. Meth. **50**, 137-140(1967).

Figure Captions

Figure 1: Plan view of the Analysis Hall at the National Superconducting Cyclotron Laboratory, Michigan State University. The neutron measurements were carried out within and outside of the shield walls of the Analysis Hall. The target position is labeled. Numbers (see Table I) label the measurement locations.

Figure 2: Cross section/elevation view of part of the K1200 cyclotron vault and the Analysis Hall. This view (the cross section A-A is defined in Figure 1) shows the position of the target and the two positions of the local and moveable iron shielding. Measurements were made at point 8* to test the effectiveness of the local shielding. The cyclotron's lower dee-stem structure is not shown. The shielding directly above the cyclotron is made from moveable iron slabs, each 30.48-cm-thick.

Figure 3: Plan view of the "catwalk" above the roof of the K1200 cyclotron (see also Fig. 2). The numbers label locations where we made neutron measurements. In the text, we distinguish these locations from points at floor level by the post-fix label "T". (This figure shows a later configuration of the beam-line in the Analysis Hall.)

Figure 4: Neutron energy spectra **F(E)xE** from a thick Hevimet target bombarded by 155 MeV/nucleon ^{4}He ions for the emission angle 94^{o} (point 9, as defined in Fig. 1).

Figure 5: The same as Figure 3, but for ^{12}C ions.

Figure 6: The same as Figure 3, but for ^{16}O ions.

Figure 7: Neutron energy spectra **F(E)xE** behind the lateral concrete shielding, from a thick Hevimet target bombarded by 155 MeV/nucleon ^{4}He ions for the emission angle 94^{o} (point 1, as defined in Fig. 1).

Figure 8: The responses of a 5-inch sphere (k_5) ("neutron flux meter") are shown as a function of <E>, for typical neutron spectra behind the biological shields of nuclear physics facilities [13, 14]. A data set of 333 neutron spectra has been used to calculated k_5 (·) as follows:

$$k_5 = \int_{E_{min}}^{E_{max}} R_5(E)\varphi(E)dE .$$

Here, $R_5(E)$ is the energy-dependent response of the detector, consisting of a 5-inch polyethylene sphere and a 4-mm x 4-mm ^{6}LiI(Eu) scintillator, and $\varphi(E)$ is the literature spectrum, where $\int_{E_{min}}^{E_{max}} \varphi(E)dE = 1$. E_{min} and E_{max} are the spectrum energy range bounds given in the literature, The value of k_5 measured in this work is shown by (●).

Figure 9: The same as in Figure 8 but for the response k_{12} of the 12-inch sphere ("neutron maximum dose equivalent meter"). The values of k_{12} (·) were calculated using

$$k_{12} = \frac{\int_{E_{min}}^{E_{max}} h(E)\varphi(E)dE}{\int_{E_{min}}^{E_{max}} R_{12}(E)\varphi(E)dE} .$$

The values of k_{12} measured in this work are shown by (●).

Figure 10: The same as in Figures 8 and 9 but for the response ratio **N(12")/N(5")** ("neutron <E> meter"). The values of **N(12")/N(5")** measured in this work are shown by (●). The ratio obtained from the PuBe-source calibration data is shown by (+).

Figure 11: The average spectrum-weighted fluence-to-dose-equivalent conversion factor <h> is shown as a function of <E>. The values of <h> are given by (•) for 330 spectra

measured at nuclear physics facilities[12], and by (o) for 52 radioisotopic neutron source spectra [15]. The values of <h> measured in this work are shown by (●). <h> is calculated using :

$$<h> = \int_{E_{min}}^{E_{max}} h(E)\varphi(E)dE \ ,$$

where φ(E) is the literature spectrum, with $\int_{E_{min}}^{E_{max}} \varphi(E)dE = 1$, E_{min} and E_{max} are the spectrum energy range bounds given in the literature. The energy dependence of the neutron maximum dose equivalent h(E) [7] is shown by (--) .

Figure 12: Neutron yields as a function of angle, $\phi(\theta)$, from a thick Hevimet target bombarded by ions of ^{4}He (■) ^{16}O(▲) and ^{12}C (●) having 155 MeV per nucleon. Fits to the equation $\varphi(\theta) = C \times \exp(-\beta\theta)$ are shown. Table 6 lists the values of the fitting parameters C and β.

Figure 13: Total neutron yields for protons and ions as a function of incident energy per nucleon: (---), (—), (o), ( ) are experimental and calculated data for protons. The references for these are cited in Ref. 2 and 17. The heavy solid line depicts data for ^{4}He ions stopping in copper. These references for these data are cited in Reference 2; The yields from the present study are shown by: ^{4}He (■), ^{16}O (▲), and ^{12}C (●).

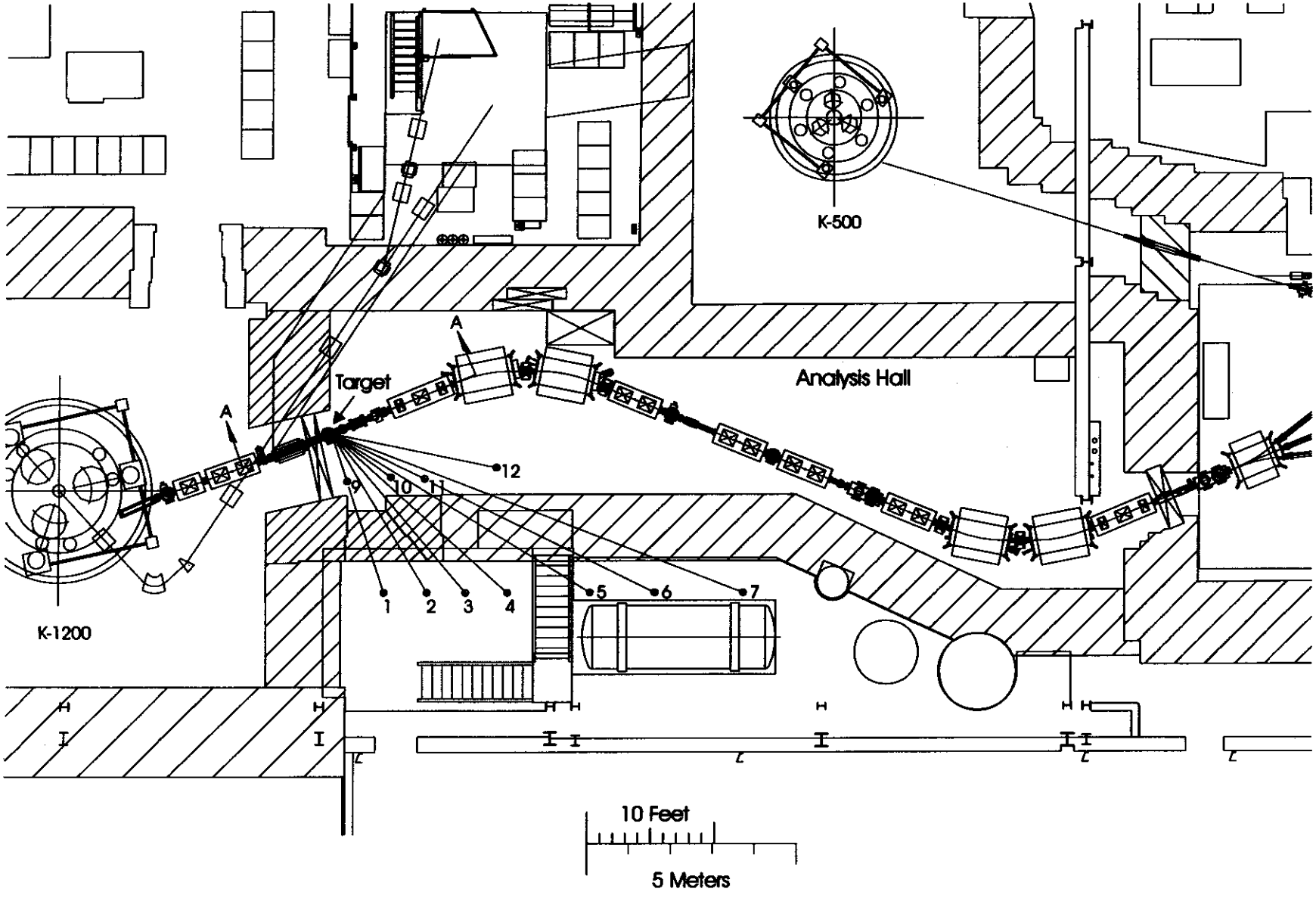
K-500
Analysis Hall
Target
A
A
12
9
10
11
1
2
3
4
5
6
7
K-1200
10 Feet
5 Meters

Figure 1

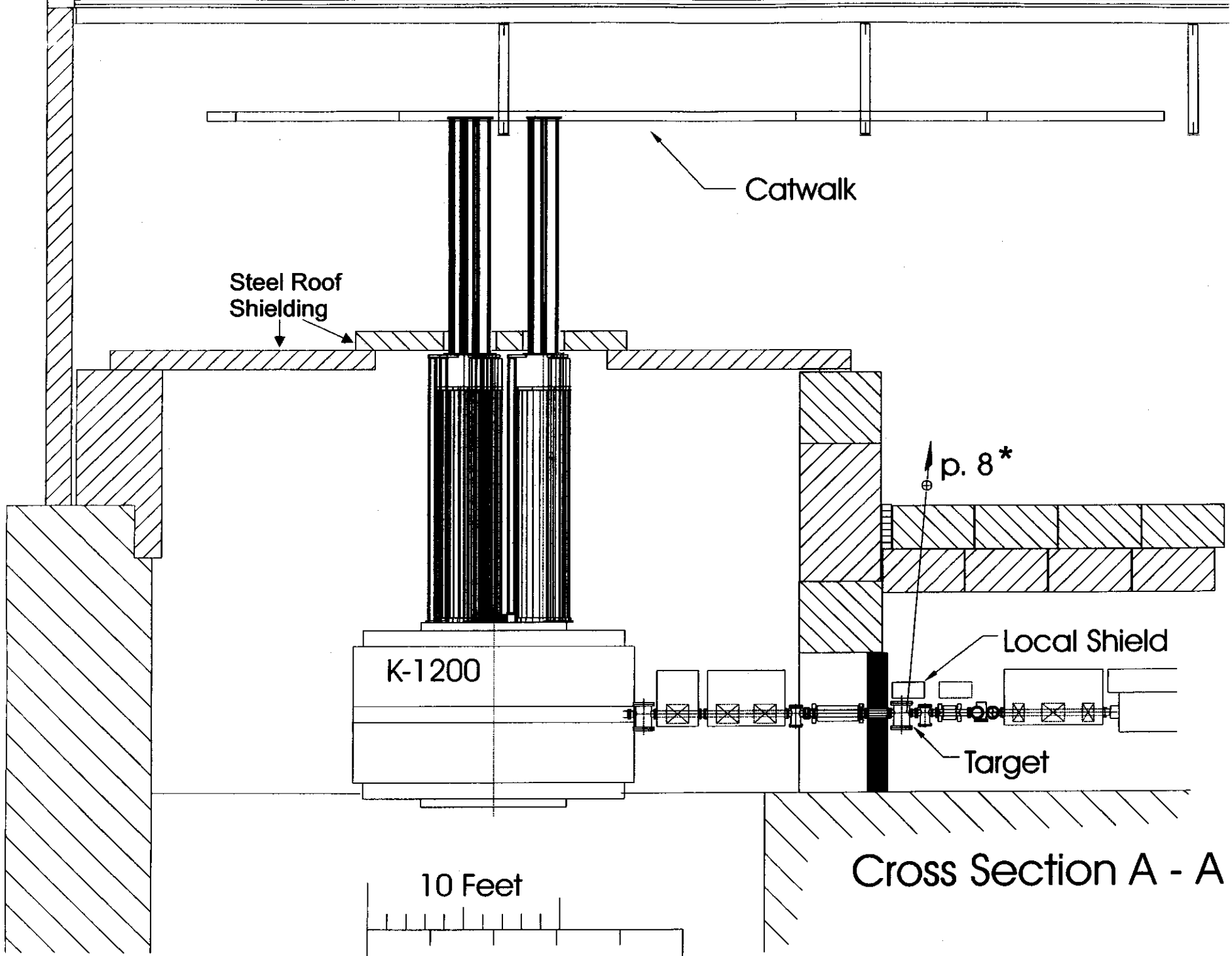
Catwalk
Steel Roof
Shielding
p. 8*
K-1200
Local Shield
Target
Cross Section A - A
10 Feet
5 Meters

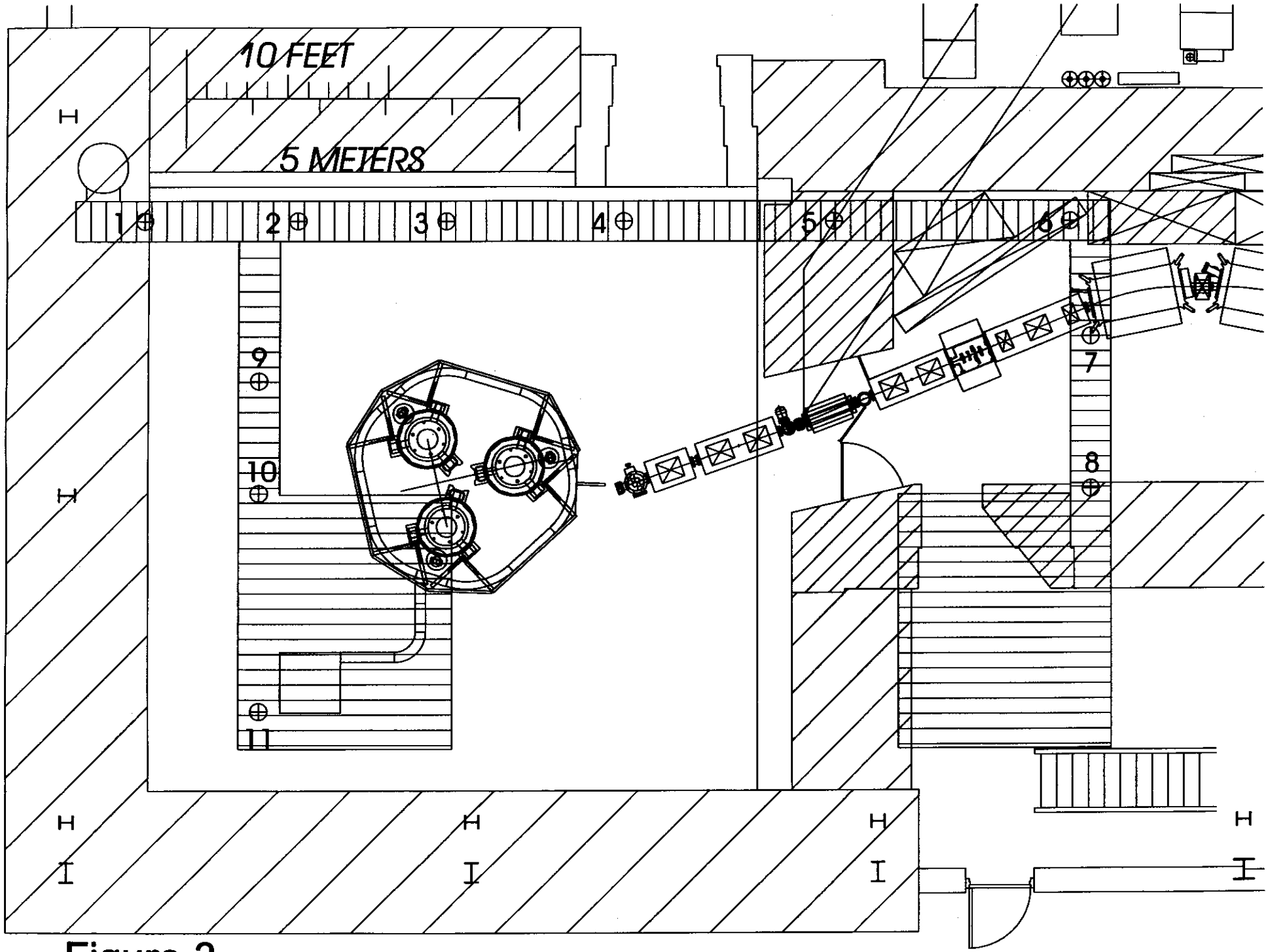

Figure 3

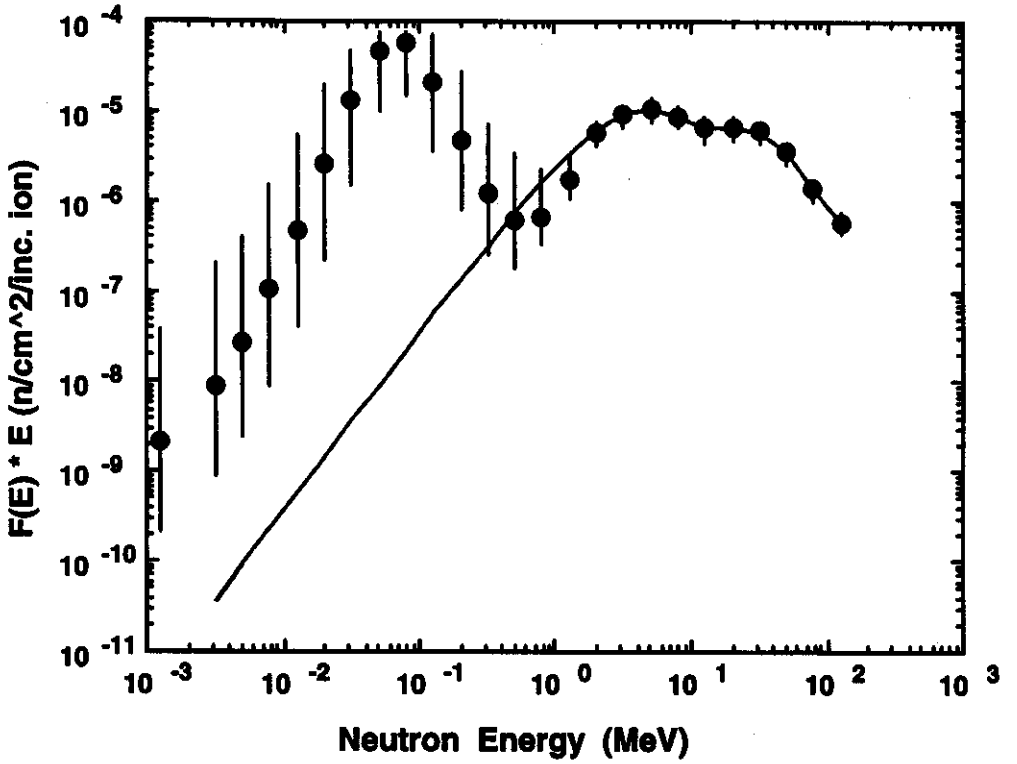
F(E) * E (n/cm^2/inc. ion)
10 -4
10 -5
10 -6
10 -7
10 -8
10 -9
10 -10
10 -11
10 -3
10 -2
10 -1
10 0
10 1
10 2
10 3
Neutron Energy (MeV)

Figure 4

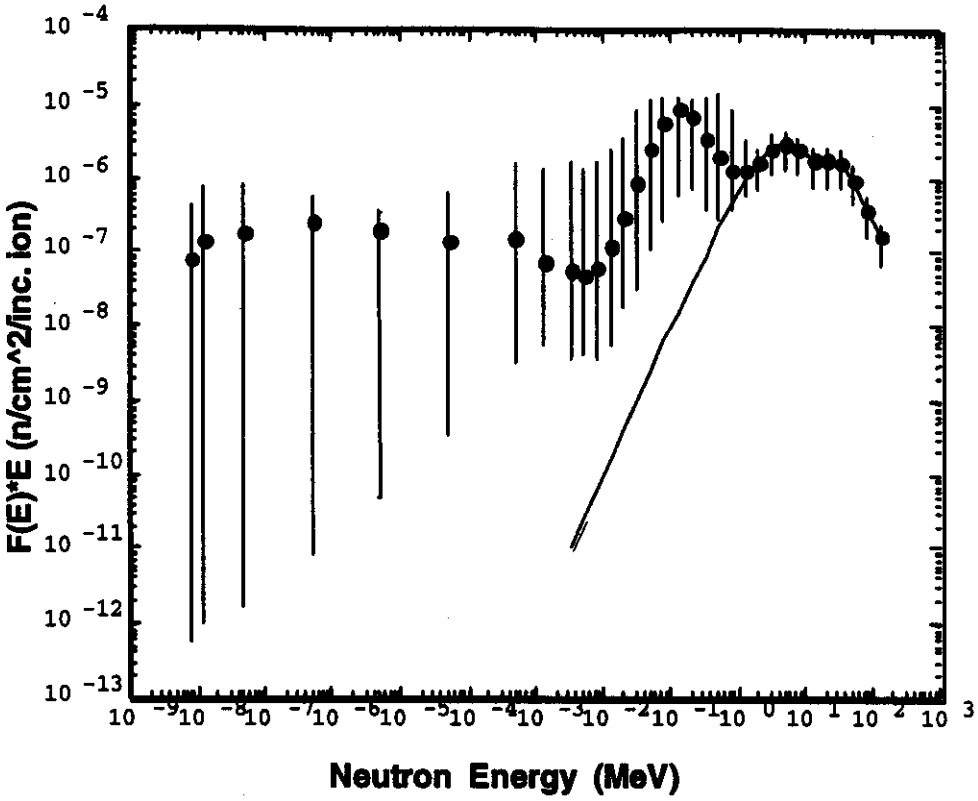

Figure 5

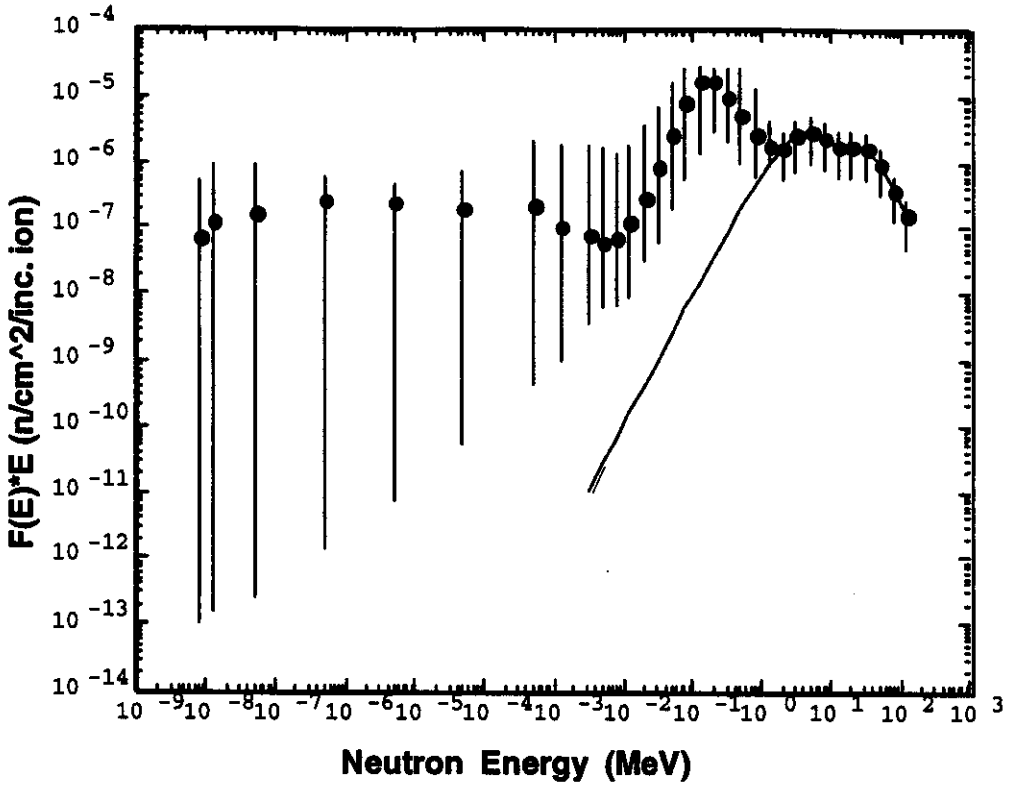

Figure 6

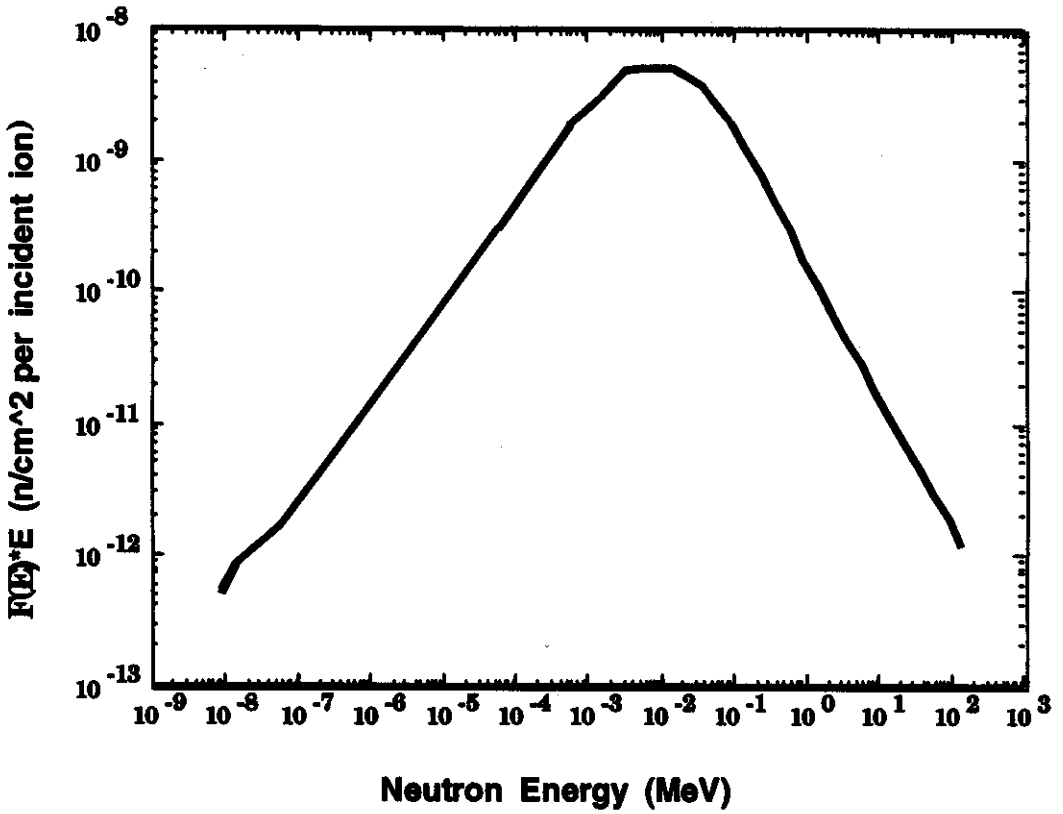
10 -8
10 -9
10 -10
10 -11
10 -12
10 -13
F(E)*E (n/cm^2 per incident ion)
10 -9
10 -8
10 -7
10 -6
10 -5
10 -4
10 -3
10 -2
10 -1
10 0
10 1
10 2
10 3
Neutron Energy (MeV)

Figure 7

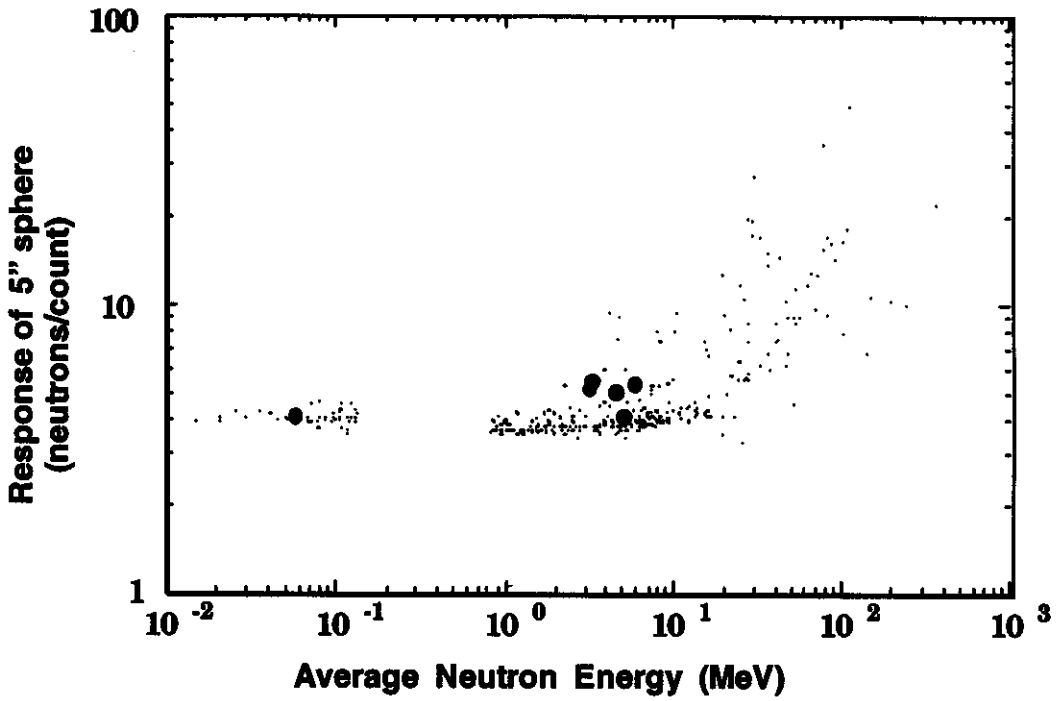
100
10
1
Response of 5" sphere
(neutrons/count)
10 -2
10 -1
10 0
10 1
10 2
10 3
Average Neutron Energy (MeV)

Figure 8

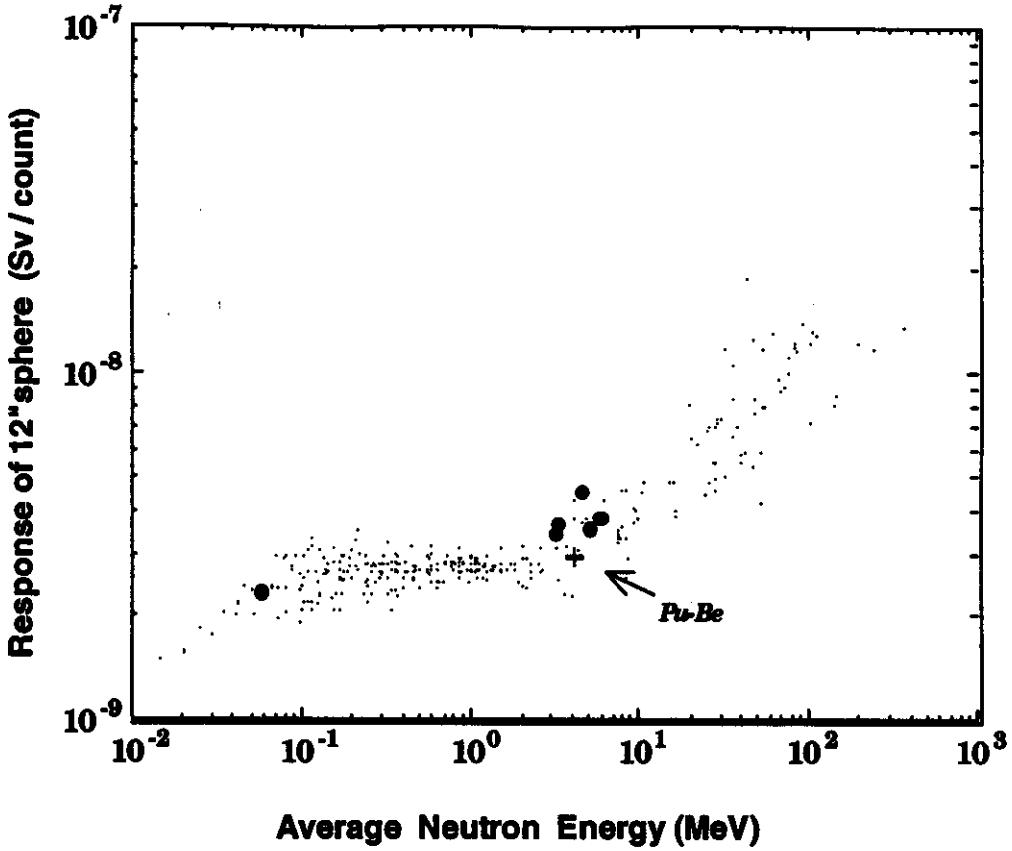
Response of 12"sphere (Sv / count)
10-7
10-8
10-9
10-2
10-1
100
101
102
103
Pu-Be
Average Neutron Energy (MeV)

Figure 9

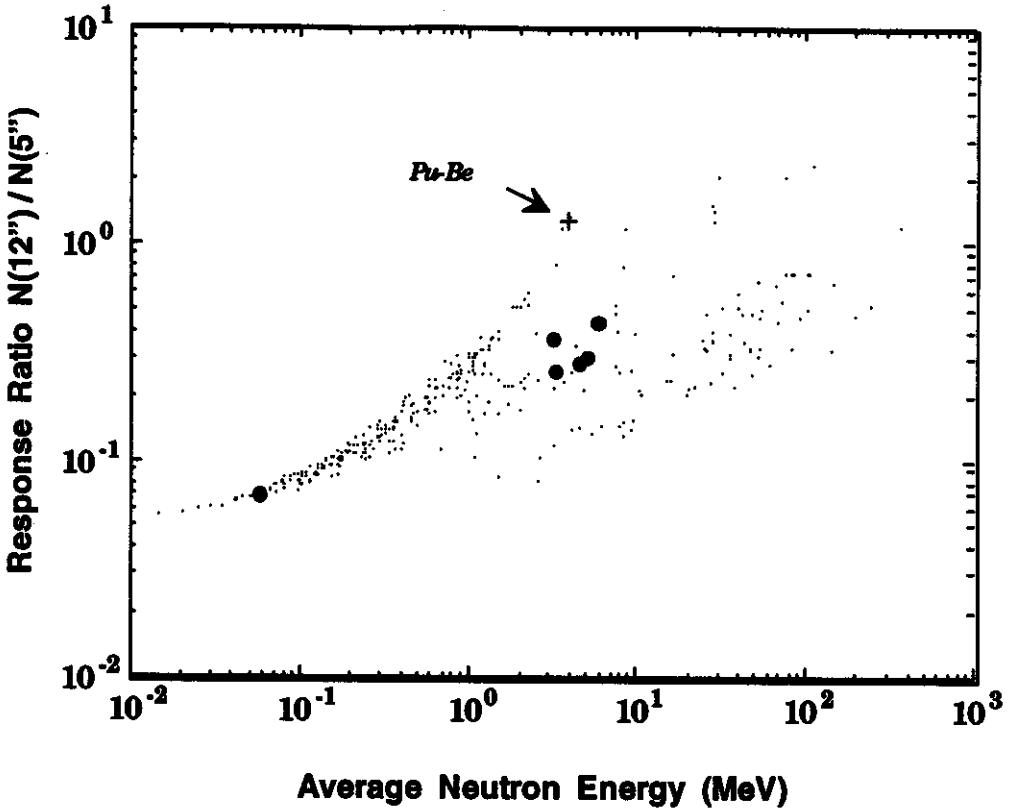
Response Ratio N(12") / N(5")
Average Neutron Energy (MeV)
Pu-Be
10^1
10^0
10^-1
10^-2
10^-2
10^-1
10^0
10^1
10^2
10^3

Figure 10

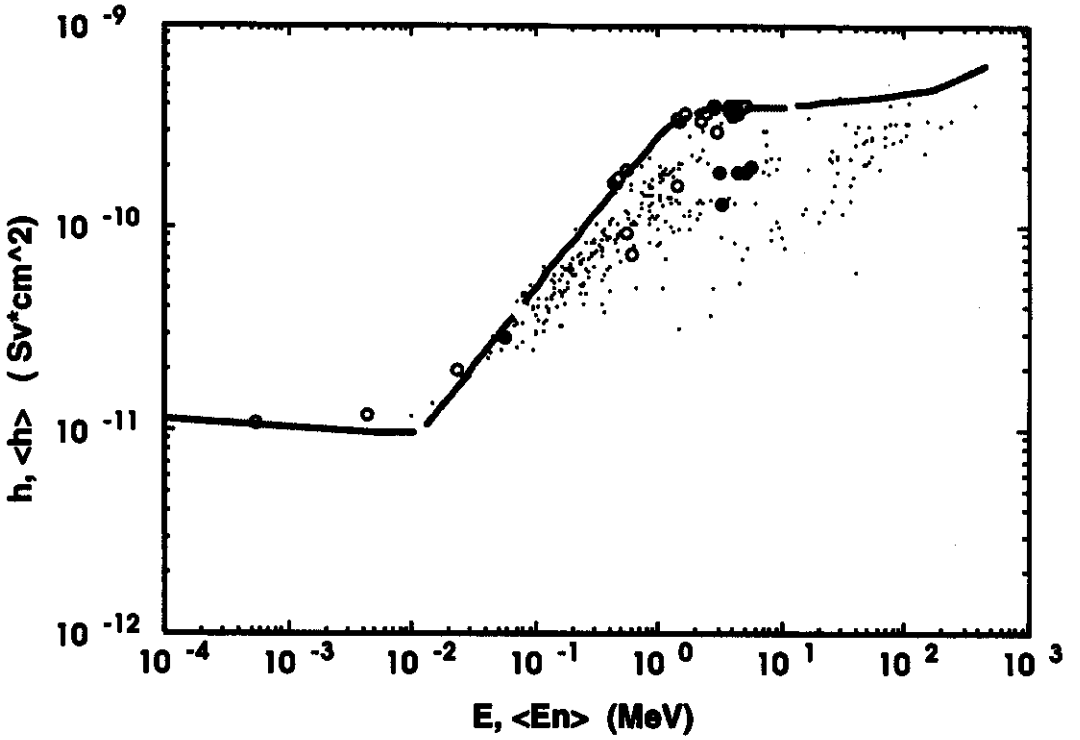
10 -9
10 -10
10 -11
10 -12
h, <h> (Sv*cm^2)
10 -4
10 -3
10 -2
10 -1
10 0
10 1
10 2
10 3
E, <En> (MeV)

Figure 11

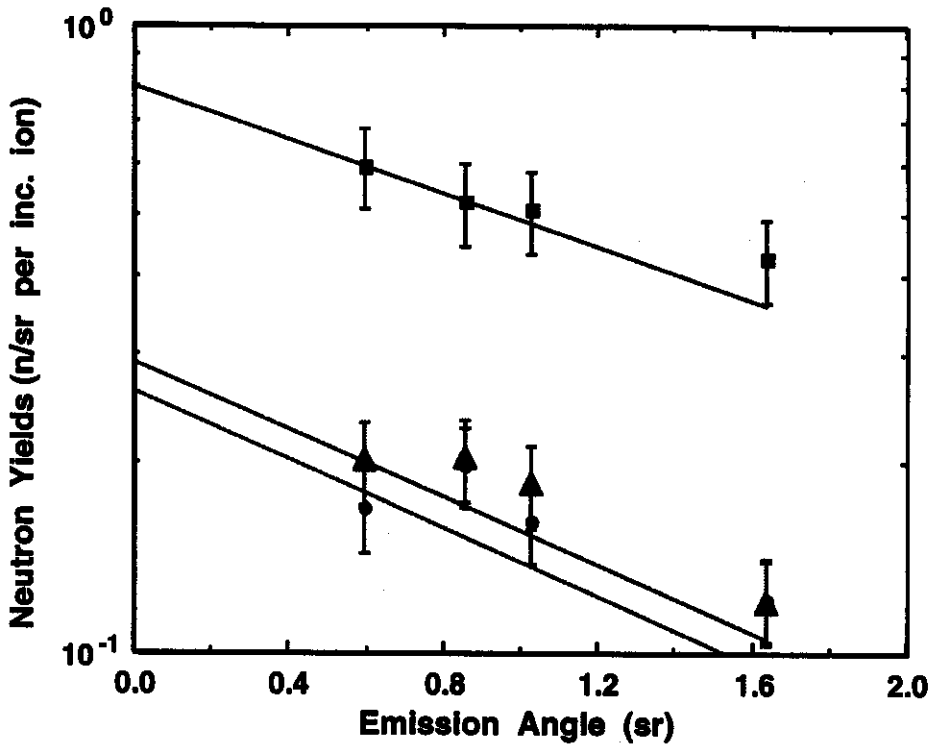
10^0
10^{-1}
Neutron Yields (n/sr per inc. ion)
0.0
0.4
0.8
1.2
1.6
2.0
Emission Angle (sr)

Figure 12

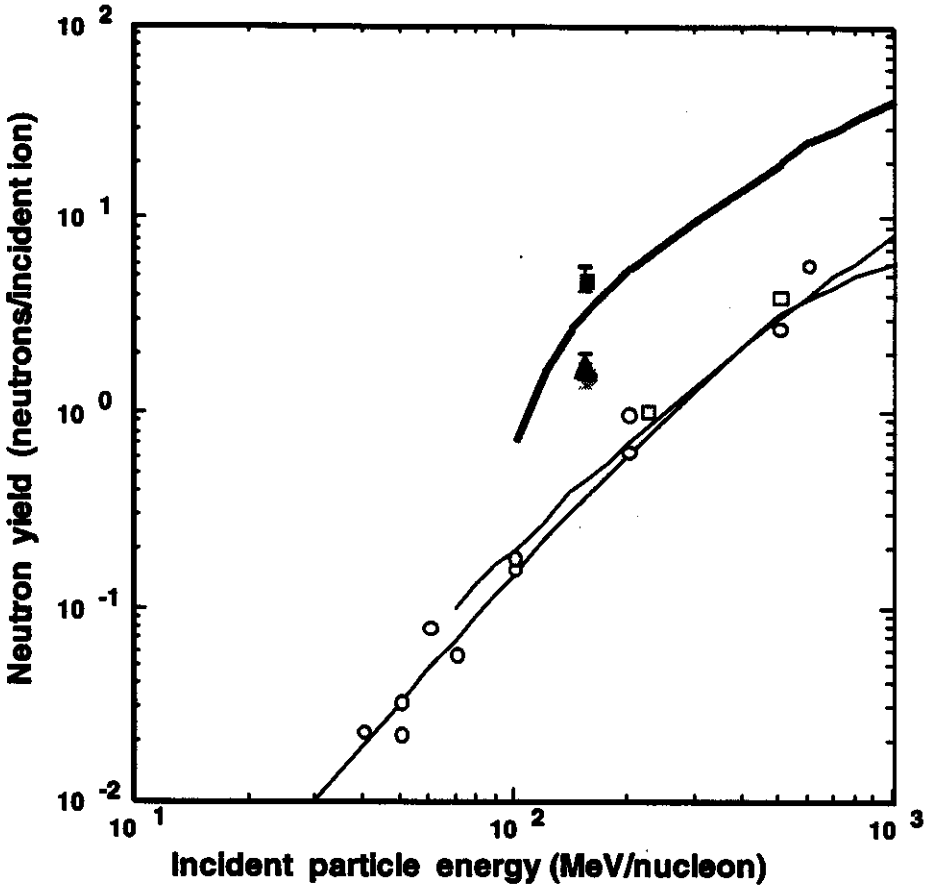
Neutron yield (neutrons/incident ion)
10 2
10 1
10 0
10 -1
10 -2
10 1
10 2
10 3
Incident particle energy (MeV/nucleon)

Figure 13